Applied Magnetic Resonance (2020) 51:1125–1143
https://doi.org/10.1007/s00723-020-01235-9

Applied
Magnetic Resonance

ORIGINAL PAPER

Capabilities of Compact High-Frequency EPR/ESE/ODMR Spectrometers Based on a Series of Microwave Bridges and a Cryogen-Free Magneto-optical Cryostat

R. A. Babunts[1] · A. G. Badalyan[1] · A. S. Gurin[1] · N. G. Romanov[1] · P. G. Baranov[1] · A. V. Nalivkin[2] · L. Yu. Bogdanov[2] · D. O. Korneev[2]

Received: 27 June 2020 / Revised: 25 July 2020 / Published online: 10 September 2020

Abstract

A magnetic resonance spectrometer operating at several fixed frequencies in the millimeter range is designed on the basis of a new generation of microwave bridges and a cryogen-free magneto-optical cryogenic system. The spectrometer allows measurements of EPR in continuous wave and pulse (free-induction decay, FID and electron spin echo, ESE) modes, photo-EPR, and optically detected magnetic resonance (ODMR) in a wide range of temperatures (1.5–300 K) and magnetic fields (up to 7 T with the ability to invert the field). It is based on a line of unified microwave bridges with a powerful oscillator and a superheterodyne receiver. Currently, they operate in W and D bands (at 94 and 130 GHz, respectively), but the frequency bands can be extended. In addition to highly stable fixed-frequency oscillators with narrow spectrum (better than − 100 dBc at 10 kHz offset at 94 GHz), they have variable frequency oscillators, which simplify tuning of the microwave circuit with a resonator and allow operation with frequency modulation when using a non-resonant microwave system. In the latter, it is possible to study large samples and quickly change the operating frequency of the spectrometer, simply replacing the microwave bridge. For all frequencies, the spectrometer uses common hardware and original software. The performance of the spectrometer at 94 GHz and 130 GHz was tested in measurements of CW-EPR, ESE and ODMR of NV defects in diamond single crystals, Tb^{3+} and Ce^{3+} ions in yttrium aluminum garnet crystals, nitrogen donors, and V^{3+} ions in 6H-SiC.

✉ R. A. Babunts
roman.babunts@mail.ioffe.ru

[1] Ioffe Institute, St. Petersburg 194021, Russia

[2] DOK Company, St. Petersburg 193318, Russia

1 Introduction

Electron paramagnetic resonance (EPR), discovered by Zavoisky in Kazan (1944) [1], is currently a powerful analytical method available for physicists, chemists, and biologists. Over 75 years, EPR and related methods played a decisive role in the study of spin phenomena in condensed matter (semiconductors and dielectrics), biophysical objects, and living systems. EPR turned out to be one of the most informative tools for non-destructive diagnostics of the structural properties of atomic and molecular objects at the electronic level.

Currently, there is growing interest in using high frequencies and strong magnetic fields in EPR spectroscopy, significantly exceeding the usual values of 9.5 GHz and 35 GHz (magnetic fields of 0.34 T and 1.25 T for $g=2$, respectively). The main advantages of high-frequency EPR are high absolute sensitivity and high spectral resolution [2–20]. Lebedev was the first who realized a high-frequency EPR spectrometer using solid-state oscillators and single-mode resonators [3, 4]. The high frequency makes it possible to detect paramagnetic centers with a large zero-field splitting and to study a wide range of correlation times of molecular motions. A number of additional benefits are provided by pulsed EPR methods at high frequencies, such as free-induction decay (FID) and electron spin echo (ESE). These methods make it possible to study spin relaxation processes to measure the relaxation times T_1 and T_2 in real time, and to separate the overlapping spectra of paramagnetic centers with different relaxation times. In combination with pulsed optical methods, it they allow to study transient processes, photo-excited particles, and excitons. Double resonances—electron-nuclear double resonance (ENDOR) and optically detected magnetic resonance (ODMR)—occupy a special place. ODMR, in which the detection of low-energy radio frequency or microwave quanta is replaced by the registration of high-energy optical quanta, and magnetic resonance manifests itself in a change in absorption or emission of light, provides a huge increase in sensitivity, as well as spatial and spectral selectivity. ODMR in some cases allows obtaining absolute sensitivity up to registration of a single spin [21–26].

The advantages of high-frequency EPR/ODMR spectroscopy are high sensitivity of EPR; achievement of sensitivity of 1000–100 spins in ODMR; high spectral resolution of EPR and ENDOR spectra; the ability to study systems with large zero-field splitting; high resolution for the study of the anisotropic properties of condensed matter and biological systems; the achievement of high Boltzmann factors, the use for the implementation of dynamic polarization of nuclei; suppression of the effects of higher order interactions; high spectral resolution in cyclotron resonance, etc.

EPR/ODMR applications include: non-destructive diagnostics of condensed matter; study of the spin properties of carriers in semiconductor systems; research and control of materials promising for use in photovoltaics; spin manipulations in spintronics and quantum information technologies, in devices based on nanostructures and single quantum objects; geological analysis; study of photosynthesis, biological processes, metalloproteins, free radicals; the development of new types of drugs; use in dosimetry; investigation of short-lived excited states, excitons, etc.

An increase in the operating frequency ω ($\omega = 2\pi\nu$) leads to a significant rise in sensitivity, i.e., a decrease in the minimum detectable concentration of spins $N_{\min}$. Indeed, $(N_{\min}/V_S) \propto \omega^{-3/2}$ provided that the sample volume V_S is proportional to the spectrometer cavity volume V_C, while the minimum number of spins is $N_{\min} \propto \omega^{-9/2}$ at a constant volume. As a rule, for small samples, the size of which cannot be increased, the filling factor is proportional to V_S/V_C ($V_C \propto \omega^{-3}$).

The spectral resolution is determined by the ability to resolve small changes in the g factor Δg, which can be written in the form $\Delta B = -\Delta g B/g$, where ΔB is the shift of the EPR line in a magnetic field with a variation of the electronic g factor Δg. This shift is proportional to the magnetic field B, which is proportional to the operating frequency in accordance with the formula $B = \hbar\omega/g\mu_B$, where μ_B is the Bohr magneton. Thus, an increase in the operating frequency of the spectrometer from the traditional X-band frequency of 9.4–94 GHz results in the increase in the resolution by a factor of 10. Subsequent increase in the frequency to 130 GHz leads to a further increase in the resolution by a factor of 1.4. At the same time, the sensitivity (for small samples) increases by a factor of $(10)^{9/2} \approx 30{,}000$, and $(1.4)^{9/2} \cong 4.5$, respectively.

An increase in the operating frequency of the EPR spectrometer also leads to the achievement of higher Boltzmann factors, which play a decisive role in many physical spin-dependent processes, including the dynamic polarization of nuclei. The high frequency makes it possible to study the EPR of spin systems with large zero-field splitting, such as, for example, non-Kramers ions, which cannot be studied using standard spectrometers operating in the X or Q bands.

In high-frequency electron-nuclear double resonance, the advantage of strong magnetic fields is manifested in the higher resolution of the Larmor frequencies of different nuclei. A shorter cavity delay time (T_c), inversely proportional to the frequency ($T_C \propto \omega^{-1}$ [2]) significantly increases the sensitivity in pulsed modes of high-frequency EPR methods.

When choosing frequency ranges for high-frequency EPR spectrometers, it is necessary to take into account that with an increase in the operating frequency above 150 GHz, the design of the device is significantly complicated and the cost increases sharply. At these high frequencies, it is necessary to use superconducting magnets with field strength above 10 T. These magnets are made in the form of a solenoid, in contrast to magnets for fields below 10 T, which can be made in the form of a split coil (such as Helmholtz rings) system. The latter are most convenient for EPR and ODMR measurements. A 275 GHz EPR spectrometer was described in [6, 7]. It uses a quasi-optical microwave unit, which is incompatible with the traditional waveguide bridges, operating at lower frequencies.

The modern development of cryogenic technology has led to the creation of closed-cycle cryomagnetic systems that do not require liquid helium and liquid nitrogen for their work and are not dependent on appropriate infrastructure. Such cryogenic systems are promising for use in magnetic resonance spectrometers (see, for example [27]).

In our previous publications [28–33], the development of high-frequency EPR/ODMR spectrometers that operate in the mm range in continuous wave (CW) and pulse modes was described. In this work, we present the EPR/ESE/ODMR

spectrometer with a line of interchangeable microwave bridges designed on a single technological platform, using standard waveguide technology and covering the frequency range up to the boundary area of application of quasi-optical technology. The spectrometer uses an autonomous closed-circle cryomagnetic system that does not require infrastructure for liquid helium and provides direct optical access to the sample. The operation of the spectrometer in various modes is demonstrated by measuring EPR, ESE, and ODMR spectra in different systems: diamond single crystal containing NV defects, yttrium–aluminum garnet (YAG) crystals dope with Tb^{3+} and Ce^{3+} ions, and 6H-SiC crystals with nitrogen donors and V^{3+} ions.

2 EPR/ESE/ODMR Spectrometer

2.1 Outline of the Spectrometer

The EPR/ESE/ODMR spectrometer is based on a series of microwave bridges and a completely autonomous cryogen-free magneto-optical system. A general view of the spectrometer is shown in Fig. 1. Its major parts, which will be described below, are: a W band (94 GHz) or D band (130 GHz) microwave bridge (1) installed in the upper part of the cryostat; a cryogen-free magneto-optical cryostat (2) with a superconducting magnet and a variable-temperature system; an optical system (3) located on an optical table and designed to excite a sample and detect luminescence; data acquisition system, temperature controller and power supply of a superconductive magnet (4); a computer (5) with an original program that monitors the operation of all components of the spectrometer and is used to collect data.

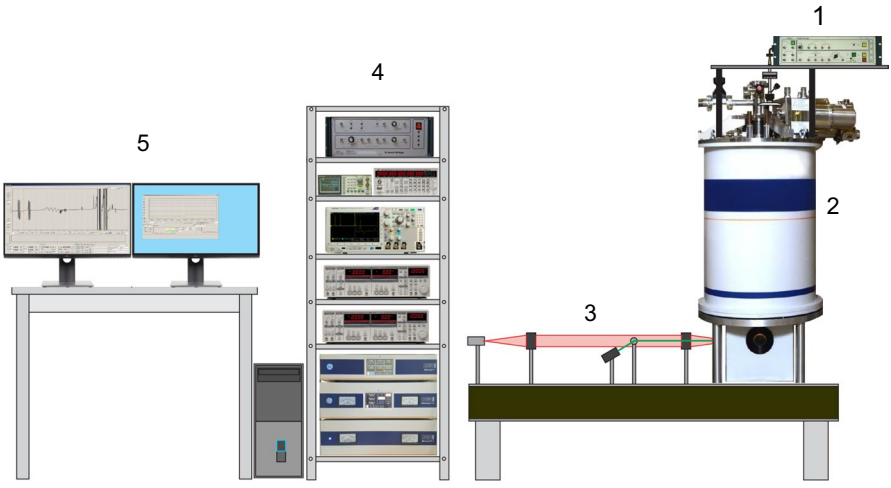

Fig. 1 General view of the EPR/ESE/ODMR spectrometer operating at 94 and 130 GHz. (1) Microwave bridge 94 GHz (or 130 GHz), (2) magneto-optical cryogenic system, (3) optical excitation and detection system on an optical table, (4) data acquisition system, temperature controller, and power supply of superconducting magnet, and (5) computer

2.2 Microwave Bridges

The basis of any EPR spectrometer is a microwave bridge, which includes an oscillator and a microwave receiver. A series of unified microwave bridges that can operate at a fixed frequency in the Q, V, W, and D microwave bands was developed as a result of collaboration of the DOK Company and the Ioffe Institute. The microwave bridges are assembled using semiconductor elements that are weakly sensitive to the magnetic field; therefore, the strong field of the superconducting magnet does not significantly affect their operation. This allows you to position the microwave bridge directly on the cryostat and minimize the length of the waveguide path, which reduces power losses. The bridges are compact and can be easily replaced depending on the experimental conditions.

Our EPR/ESE/ODMR spectrometer uses microwave bridges of W and D bands. They operate at 94 and 130 GHz, respectively. A simplified diagram of a microwave bridge is presented in Fig. 2a. Photographs of the microwave bridges 94 GHz and 130 GHz are shown in Fig. 2b and Fig. 2c, respectively.

The microwave bridge contains a highly stable solid-state oscillator with a fixed frequency of about 7.2 GHz, the output signal of which is supplied to the frequency multipliers by N in the transmitter channel and by $(N-1)$ in the receiver channel. A frequency conversion with a multiplication factor of $N=13$ is used to obtain the frequency of 94 GHz and $N=18$ to obtain the frequency of 130 GHz. The high-frequency signal is amplified and passed via an attenuator, modulator, and circulator to the microwave insert and to the sample. The output frequency of the microwave oscillator has a very-low-phase noise and narrow spectrum.

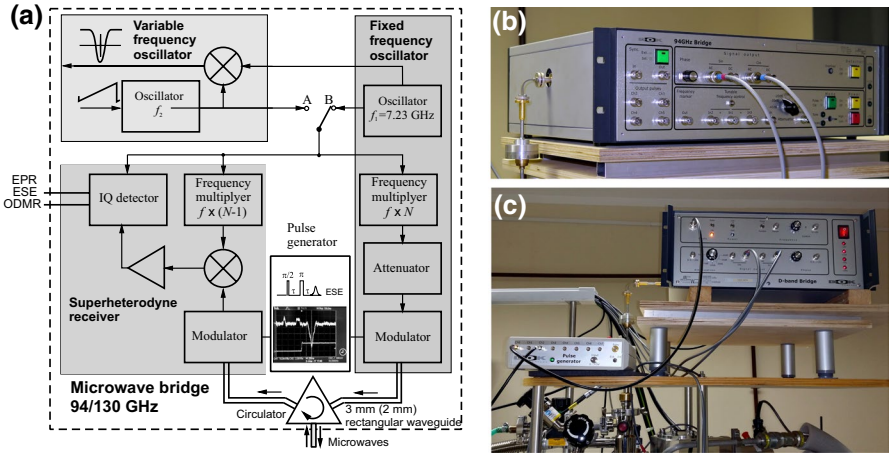

Fig. 2 **a** A simplified scheme of the microwave bridge. The bridges 94 and 130 GHz differ by a multiplication factor N of the master oscillator frequency of about 7.2 GHz. The bridge includes a fixed-frequency oscillator, a variable frequency, voltage-controlled oscillator, a superheterodyne receiver, an IQ detector, modulators, a programmable, multichannel pulse generator, and a frequency-mark former. **b**, **c** Photographs of the W band (94 GHz) and D band (130 GHz) microwave bridges, respectively

A sensitive superheterodyne receiver and a quadrature (IQ) detector are used in the microwave bridges. The signal reflected from the sample is fed to the circulator and the mixer of a receiver, after which the intermediate-frequency signal is amplified and fed into IQ detector.

The modulators are necessary for the spectrometer operation in pulsed regimes, in particular, with ESE signal detection. The operation of modulators is controlled by a programmable, multichannel pulse generator that produces a desirable sequence of pulses and prohibits the receiver switching on when the transmitter is operating. The pulse duration can be varied from 10 ns to 0.1 s in increments of 3.2 ns.

In addition to the highly stable fixed-frequency oscillator the microwave bridge contains a tunable oscillator with a voltage-controlled frequency. Its tuning range is ± 0.25 GHz. A method of the cavity tuning is new for the mm-wave bridges. In the regime of tuning, the oscillator switch is in position *A* that ensures observation of a resonance curve of the working cavity and the signal ("mark") of beats between the two oscillators, which is formed on the high-frequency mixer at the moment of coincidence with the main oscillator frequency. The cavity can be tuned to the "mark"—that is, to the main oscillator frequency. After this, the switch is set to position *B* (measurement regime), where only the highly stable oscillator operating at a fixed frequency is employed. A variable frequency oscillator can also be used to register CW-EPR with frequency modulation instead of field modulation.

Measurements with a highly stable fixed-frequency oscillator that has a narrow spectrum (below -100 dBc at a 10 kHz offset at 94 GHz) and extremely high-frequency stability (better than 10^{-6}) allow recording of EPR lines with a width of up to microtesla. Since the operating frequency of the spectrometer is fixed, its measurement at each recording and correcting the EPR spectra to the same frequency are not required.

2.3 Cryogen-Free Magneto-Optical System

We use the magneto-optical Cryofree® superconducting magnet system SpectromagPT from Oxford Instruments. It has a split-coil superconducting magnet creating a horizontal magnetic field up to 7 T that is sufficient to study EPR, ESE, and ODMR in W and D bands. The magnetic field can be scanned over the entire range, without worrying about the increased consumption of liquid helium, as is the case with conventional cryostats. It is possible to record spectra with field inversion and a smooth transition through the zero field. This is important for studying EPR of many impurity ions in solids, for example, rare-earth ions in garnets. The field can be quenched at any value.

The cryomagnetic system provides a wide range of sample temperatures from 1.5 to 300 K and high-temperature stability. Optical access through four windows allows you to work in Faraday (longitudinal magnetic field) and Voigt (transverse magnetic field) geometry and register photo-EPR and ODMR via the intensity and polarization of luminescence, Faraday rotation, magnetic circular dichroism (MCD) in absorption, to study level anticrossings, etc.

2.4 Microwave Insert

A low-temperature microwave insert can be made in two versions: (1) a non-resonant system in which a sample is placed on the closed end of a cylindrical waveguide, and (2) a microwave system with a single-mode resonator. At this stage, we use mainly a non-resonant system. Figure 3 shows a general scheme of the magneto-optical cryostat (a) and the microwave system (b) that is inserted into the variable-temperature volume of the cryostat. The microwave power from the microwave bridge, which is installed directly above the cryostat, is supplied to the sample. The sample inside the waveguide is placed in the center of the split-coil superconducting magnet.

The microwave insert is equipped with heat shields, thermo-stabilizer, and modulation coils, which create an alternating magnetic field on the sample. Microwave energy from the microwave bridge enters a rectangular waveguide, then through a vacuum seal, and the transition from a rectangular to a circular waveguide is supplied to the upper part of the circular waveguide. A circular waveguide with an inner diameter of ca. 5 mm is used. Through a rotating joint with a goniometer, it is directed to the stainless steel circular waveguide, at the end of which the sample is placed. The circular waveguide, together with the wires leading to the temperature sensor, temperature stabilizer heater, and modulation coils, passes into the cryostat. For optical access to the sample in photo-EPR and ODMR experiments, horizontal slits opposite to the sample were sawn in the cylindrical waveguide.

Using a non-resonant microwave insert provides a possibility to study large samples (up to some mm in size) and working with short pulses (down to 10 ns) for measuring ESE of paramagnetic centers with short relaxation times T_1 and T_2. It allows applying several frequencies to the sample for detecting ODMR, "hole" burning in ODMR, electron–electron double resonance (EEDR), and dynamic nuclear polarization. The same microwave insert can be used both with the 94 GHz and 130 GHz bridges. It is possible to easily change the operating frequency of the spectrometer: 94 GHz or 130 GHz thanks to a unified circuit for connecting microwave bridges to the microwave insert. In CW-EPR measurements, the sensitivity of the spectrometer with the non-resonant microwave system shown in Fig. 3b, estimated using standard samples, is of the order of 10^{10} spin/mT per a single record.

2.5 Optical System

The optical system of the spectrometer is designed to irradiate the sample with light when recording EPR (photo-EPR) and for studying ODMR. Its configuration is flexible and strongly depends on the system under study. Figure 1 shows the simplest version of the optical system in which magnetic resonance is detected by variations in the luminescence intensity excited by a laser. Such a scheme was used to detect ODMR of NV defects in diamond.

By changing the configuration of the optical system of the spectrometer, it is possible to study photo-EPR, ODMR, optically detected level anticrossings, etc.

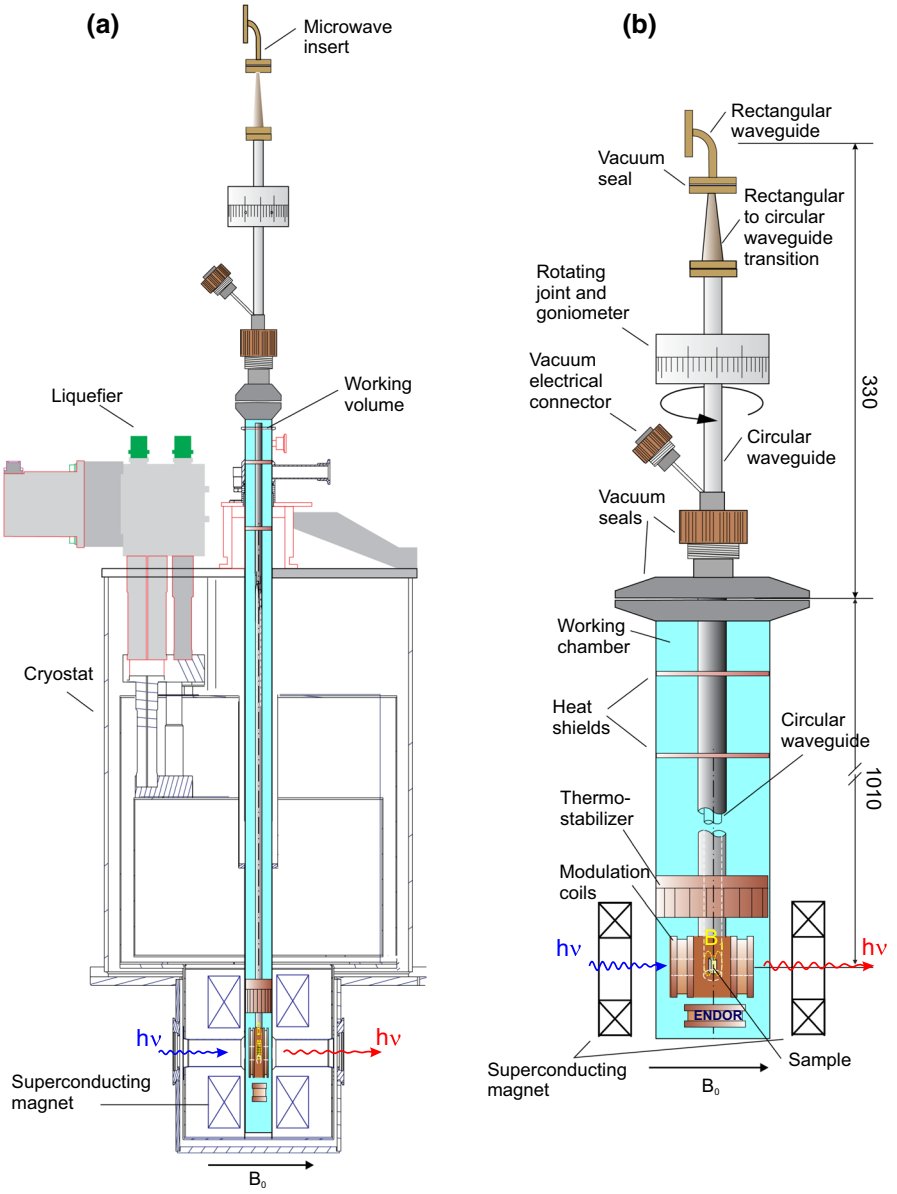

Fig. 3 **a** A scheme of the magneto-optical cryostat with a split-coil superconducting magnet and a microwave system inserted into the variable-temperature volume. **b** The design of a non-resonant microwave system equipped with heat shields, thermo-stabilizer, and modulation coils which create an alternating magnetic field on the sample placed inside the circular waveguide

The system can work in the geometry of Faraday (longitudinal magnetic field) and Voigt (transverse magnetic field). ODMR can be recorded via intensity or circular polarization of luminescence, magnetic circular dichroism in absorption, and Faraday rotation.

It is known that during the operation of cryogen-free cryomagnetic systems, vibrations occur. They appear primarily in ODMR, but their impact can be reduced by averaging. In our measurements of ODMR in diamond described in Sect. 3.1, the effect of vibrations was not critical.

2.6 Spectrometer Electronics and Software

CW-EPR is recorded with modulation of the magnetic field at audio frequency. Two lock-in amplifiers are used to detect signals from the outputs of the IQ detector. Modulation of the magnetic field is carried out using a low-frequency oscillator connected to modulation coils. The same oscillator is used as a source of control voltage for recording spectra with microwave frequency modulation. In pulse spectrometer mode, a digital oscilloscope is used to detect FID and ESE signals.

All electronic equipment is connected to a computer. A special original program controls the operation of the spectrometer and is used for data acquisition. The program has a convenient interface as shown in Fig. 4a and can simultaneously display multiple spectra. It constantly monitors all the basic parameters of the spectrometer and cryogenic system with recording LOG files. The program automatically saves the spectra in simple and convenient ASCII format. Using macros, you can carry out some routine operations, for example, recording orientation and temperature dependencies.

In pulsed mode, operation of the microwave bridge is controlled by a programmable, multichannel pulse generator and signals are detected by a digital oscilloscope. The program interface for setting the pulse sequence is shown in Fig. 4b. Figure 4c is a screenshot of an oscilloscope showing a three-pulse sequence and signals of a stimulated electron spin echo. You can program up to eight channels, each of which can contain up to eight pulses. Therefore, we can control the operation of the microwave oscillator, and the receiver and external equipment, such as, for example, a laser. The duration of each pulse can be chosen from 10 ns to 100 ms with a step of 3.2 ns. There are predefined schemes of the main pulse sequences: 1 pulse—for free-induction decay, 2 pulses—for the Hahn echo, and 3 pulses—for the Mims echo. In the latter, it is possible to apply a radio frequency pulse between the second and third microwave pulses. There are also patterns. There are also templates for the Devis pulse sequence and for relaxation time measurements.

There is protection against simultaneous switching on the receiver and the microwave bridge. In addition, it is possible to adjust the phases of the signal from the IQ receiver digitally after recording the spectrum. The program also provides the ability to record ESE-detected ENDOR spectra using linear and stochastic regimes. Remote control of the spectrometer is possible.

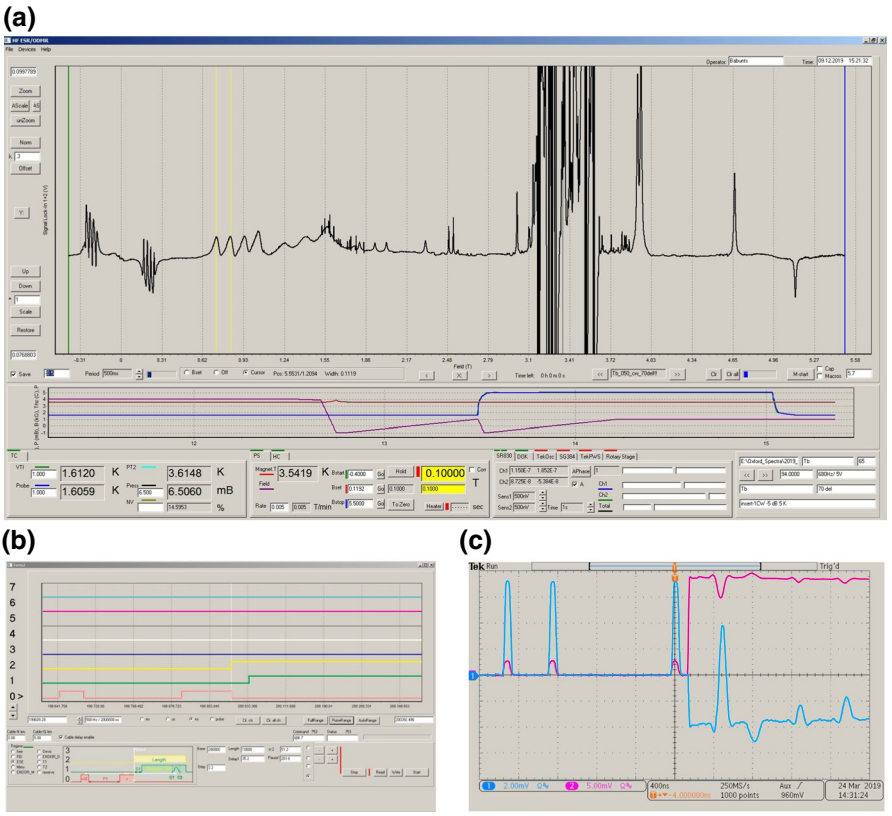

Fig. 4 **a** Interface of the program that controls the spectrometer in CW and pulse modes and is used for data acquisition; **b** a window for setting up the pulse sequence; **c** a screenshot from the oscilloscope showing a three-pulse sequence and signals of the stimulated electron spin echo

2.7 Technical Specification of the Spectrometer

The main technical data of the spectrometer are summarized in the table.

Operating modes	CW-EPR, Pulse EPR (FID, ESE), photo-EPR, ODMR, ENDOR (under development) Low-frequency modulation of the magnetic field or microwave frequency	
Microwave bands	W	D
Fixed frequency oscillator	94 GHz	130 GHz
Variable frequency oscillator	94 ± 0.25 GHz	130 ± 0.25 GHz
Maximum output power in pulsed mode	100 mW	50 mW
Maximum attenuation	40 dB40 dB	40 dB
Microwave pulse duration	10 ns–100 ms	
Pulse duration increment	3.2 ns	
Repetition rate	0.1–10 000 Hz	

Number channels of a pulse generator	8
Microwave insert	A non-resonant system or a system with a resonator
Magneto-optical system	A closed-circle magneto-optical cryostat with horizontal magnetic field and four windows
Magnetic field	−7 to +7 T
Magnetic field resolution	0.05 mT
Magnet energisation rate	0.1–0.001 T/min
Operating temperature range	1.5–300 K
Diameter of the variable-temperature volume	30 mm

3 Performance of the Spectrometer

The spectrometer performance was verified by measurements spectra of EPR, ESE, and ODMR at 94 GHz and 130 GHz in four different systems: diamond single crystals with NV defects, yttrium aluminum garnet crystals doped with Tb^{3+} and Ce^{3+} ions, 6H-SiC crystals with nitrogen donors, and 6H-SiC with V^{3+} ions.

3.1 ODMR of NV Defects in Diamond Crystals

In systems based on spin color centers in diamond and silicon carbide, which are promising for applications in sensorics and for creating the elemental base of quantum computing, ODMR is especially promising to detect small spin ensembles up to one spin [34].

The performance of the spectrometer in ODMR experiments is illustrated by measurements of the ODMR spectra of NV defects in diamond. ODMR was recorded as microwave-induced variations of the PL intensity using modulation of the magnetic field or microwave frequency at low frequency and a lock-in amplifier. A non-resonant microwave system was used; optical access to the sample was provided by horizontal slots located opposite the sample in a cylindrical waveguide. Luminescence of NV defects was excited with a 532 nm laser, selected with glass filters and detected by a PM tube.

Figure 5a shows 130 GHz ODMR spectra in a diamond single crystal containing NV centers. The spectra were recorded with magnetic field modulation at a temperature of 10 K and different orientations of the crystal in the magnetic field. The modulation frequency was 680 Hz and the amplitude was ~ 0.1 mT. The rotation of the crystal was carried out around an axis close to the <110>, that is, to the edge of the crystal; deviation from the <110> direction was several degrees.

In the general case, the EPR spectra of NV centers are described by a standard spin Hamiltonian:

$$\hat{H} = \mu_B B \times g \times S + S \times D \times S + S \times A \times I + g_I \mu_N B \times I + I \times Q \times I, \quad (1)$$

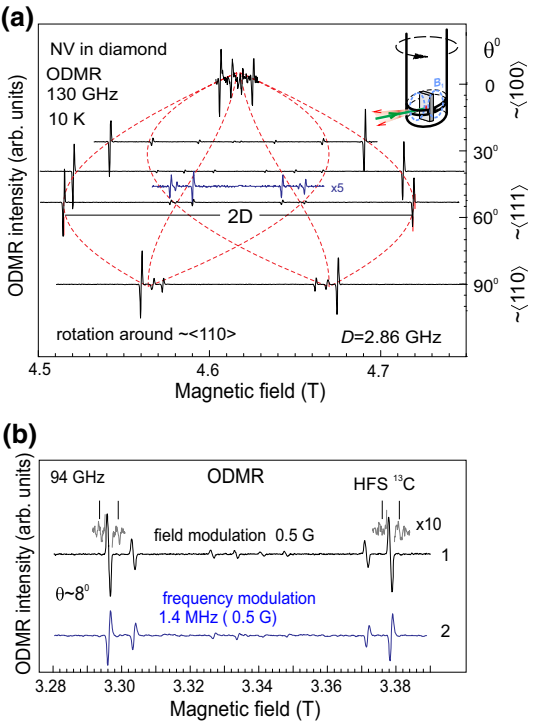

Fig. 5 **a** ODMR spectra at a frequency of 130 GHz recorded via the luminescence intensity of NV centers in a diamond single crystal at a temperature of 10 K for different orientations of the sample in magnetic field. The rotation axis was close to <110> (the deviation from <110> was several degrees). Luminescence was excited by a 532 nm laser, the magnetic field modulation frequency was 680 Hz, the modulation amplitude ~0.1 mT. Dashed lines show the calculated angular dependences. **b** 94 GHz ODMR spectra of NV centers in diamond recorded with magnetic field modulation (1) and frequency modulation (2) at a temperature of 20 K and the magnetic field orientation ca. 8° with respect to the *c* axis. Modulation frequency was 680 Hz in both cases, the magnetic field modulation amplitude was 0.05 mT, and the frequency modulation amplitude was ~1.4 MHz (which corresponds to magnetic field modulation amplitude of 0.05 mT). Vertical lines mark the hyperfine structure lines that are due to the hyperfine interaction with the nucleus of the ^{13}C isotope located in one of the three nearest carbon positions

where the first term is the Zeeman electron spin interaction; the second term refers to the fine-structure splitting and can be written as $D[S_z^2+S(S+1)]+E(S_x^2-S_y^2)$; the third term describes the hyperfine interaction (HFI); the fourth term represents the Zeeman nuclear interaction, and the fifth term represents the quadrupole interaction. Since only the first and fourth terms of the spin Hamiltonian depend on the magnetic field, EPR measurements at different frequencies allow us to separate these interactions and correctly describe the corresponding paramagnetic centers. For NV centers, $S=1$. Dashed lines in Fig. 5a present the angular dependences calculated using (1) with the parameters from [35] for the ground state of the NV centers, taking into account the four magnetically nonequivalent orientations of NV centers with the axes along <111> directions.

Figure 5b shows 94 GHz ODMR spectra of NV centers recorded at a temperature of 20 K with modulation of the magnetic field (1) and modulation of the microwave frequency (2) at 680 Hz. The amplitudes of modulation were ~0.05 mT and ~1.4 MHz, respectively. Modulation of the operating frequency of 94 GHz with an amplitude of 1.4 MHz corresponds to the magnetic field modulation amplitude of 0.05 mT (1 mT corresponds to 28 MHz for $g=2.0$). The ODMR signals belong to NV centers, which axes are directed along <111> axes of the crystal. The weak satellite lines marked by arrows represent the components of the hyperfine structure (HFS), which is due to the interaction of the unpaired electron with the nucleus of the ^{13}C isotope located in one of the three nearest carbon positions.

3.2 CW-EPR of Tb^{3+} and Ce^{3+} in Yttrium Aluminum Garnet

The EPR spectra in Fig. 6 are a demonstration of the capabilities of the spectrometer for detecting paramagnetic centers with giant zero-field spitting, the so-called, non-Kramers ions, which have an even number of electrons. Tb^{3+} ions in YAG have zero-field splitting close to 3 cm^{-1}, therefore, to study EPR of these ions, a frequency close to 100 GHz is necessary [31]. Figure 6a shows the CW EPR spectra of YAG:Ce,Tb crystals measured at 94 GHz with different registration modes: low-frequency modulation of the magnetic field with an amplitude of ~0.1 mT, and modulation of the operating frequency ν with an amplitude of ~2.5 MHz. The modulation frequency was 680 Hz. EPR signals of Ce^{3+} and Tb^{3+} are observed in a very large range of magnetic fields. Mo^{3+} is a trace impurity. The relationship between the change in the energy of the microwave quantum caused by the modulation of the operating frequency $\delta E = h\delta\nu$ and the corresponding change in the position of the resonance in the magnetic field δB is shown as an inset. Since Tb nuclei have a spin of 3/2, four hyperfine structure lines are observed in their EPR spectra.

Figure 6b shows the calculated energy-level scheme of Tb^{3+}centers in YAG crystal for $B \parallel [100]$ and EPR transitions at 94 GHz and 130 GHz. The 94 GHz and 130 GHz CW-EPR spectra, shown in the lower part of the figure, allowed to reveal four types of Tb^{3+} centers Tb^{3+}(I), Tb^{3+}(II), Tb^{3+}(III),Tb^{3+}(IV), which differ in the zero-field splitting [36]. EPR spectra of Tb^{3+}(III) and Tb^{3+}(IV) centers, for which $\Delta > 94$ GHz, cannot be observed at 94 GHz but they were detected at 130 GHz.

94 GHz EPR signals at $B=0$ belong to Tb^{3+}(II)—centers for which $\Delta \approx 94$ GHz. These signals recorded with modulation of the microwave frequency are much more intense than those obtained with magnetic field modulation, since the slope of the Tb^{3+} energy levels near $B=0$ is weak, and frequency modulation leads to a larger effective value of δB.

3.3 CW-EPR of Nitrogen Donors N in 6H-SiC Crystal

Nitrogen donors in 6H-SiC can occupy different positions in the crystal lattice: hexagonal (h) and two quasicubic ($k1$, $k2$). The first EPR studies on N donors in SiC were done in [36]. A review of electronic properties of N donors obtained by EPR and ENDOR at 9.5 GHz was presented in [37]. Observation of high-frequency EPR

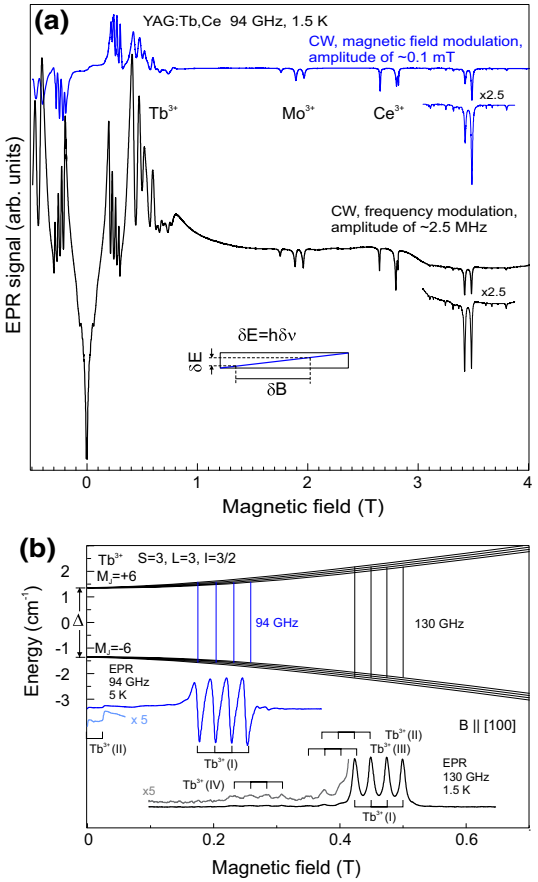

Fig. 6 **a** 94 GHz EPR spectra in YAG crystal doped with rare-earth elements Tb^{3+} and Ce^{3+} (Mo is a trace impurity) recorded with ~0.1 mT magnetic field modulation (1), and with frequency modulation (2). The modulation frequency was 680 Hz, the modulation amplitudes were ~0.1 mT and ~ 2.5 MHz, respectively. The magnetic field was directed at about 25° relative to a [100] axes of the crystals. The relationship between energy variations due to modulation of the operating frequency modulation, $\delta E = h\delta\nu$, and the corresponding change in the position of the resonance line δB is shown in the inset **b**. Calculated energy levels of Tb^{3+} centers in YAG crystal for $B \parallel [100]$ with EPR transitions at 94 GHz and 130 GHz. CW-EPR spectra recorded at 94 GHz and 130 GHz, respectively, are shown below. Positions of EPR lines that belong to Tb^{3+}(I), Tb^{3+}(II), Tb^{3+}(III), and Tb^{3+}(IV) centers are marked. EPR spectra of Tb^{3+}(III) and Tb^{3+}(IV) centers are not observed at 94 GHz, since for these centers, Δ exceeds the energy of the microwave quantum

at 142 GHz [38] allowed to separate overlapping EPR lines due to the high spectral resolution and attribute them to specific positions of nitrogen in the SiC lattice. Electronic structure of N donors in SiC have been studied by EPR and ENDOR in X and Q bands [39] and in W band [40, 41].

Figure 7 presents CW-EPR spectra of shallow nitrogen donors in 6H-SiC, measured at three frequencies: 9.5 GHz (X band), 94 GHz (W band), and 130 GHz (D band) for $B \parallel c$ and $B \perp c$. The inset shows the crystal structure of 6H-SiC. Three

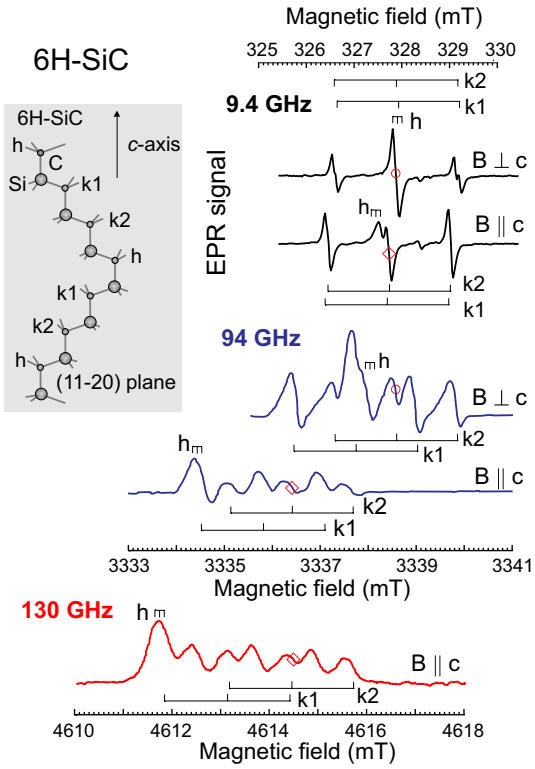

Fig. 7 CW-EPR spectra of shallow nitrogen donors in a 6H-SiC crystal, measured at three frequencies: 9.5 GHz, 94 GHz, and 130 GHz for two extreme orientations of magnetic field $B \parallel c$ and $B \perp c$. The inset shows the crystal structure of 6H-SiC and three positions of the nitrogen donors in the lattice: hexagonal (h) and two quasicubic (k_1, k_2). EPR lines of N donors in these positions are marked

different positions of nitrogen in the crystal are marked—a hexagonal (h) and two quasicubic ($k1$, $k2$). The 6H-SiC crystal consists of tetrahedra with four bonds per atom. Two bonds lie in the plane of the figure ($11\bar{2}0$) and a staircase pattern is formed parallel to the direction of the c axis. For 6H-SiC, this leads to three nonequivalent positions $k1$, $k2$, and h. N donors in these positions differ in g-factors and HFI constants [38–42].

It can be seen from Fig. 7 that measurements at high frequencies make it possible to separate different nitrogen positions due to the difference in g factors, as well as to distinguish between different orientations of paramagnetic centers. The hyperfine splitting due to interaction with the nitrogen nucleus ($I=1$) does not depend on frequency, i.e., on the magnetic field, as it follows from the spin Hamiltonian (1).

3.4 EPR and ESE of V^{3+} in 6H-SiC

Vanadium doping of SiC is one of the main methods for the production of semi-insulating substrates required for high-power microwave devices. EPR spectra of vanadium in SiC were first obtained in [43] where its charge state was identified. V^{3+} ions have a $3d^2$ electronic configuration, a spin $S=1$, and a nuclear spin $I=7/2$ (100%). Figure 8a shows CW-EPR spectra in 6H-SiC:V crystal, measured

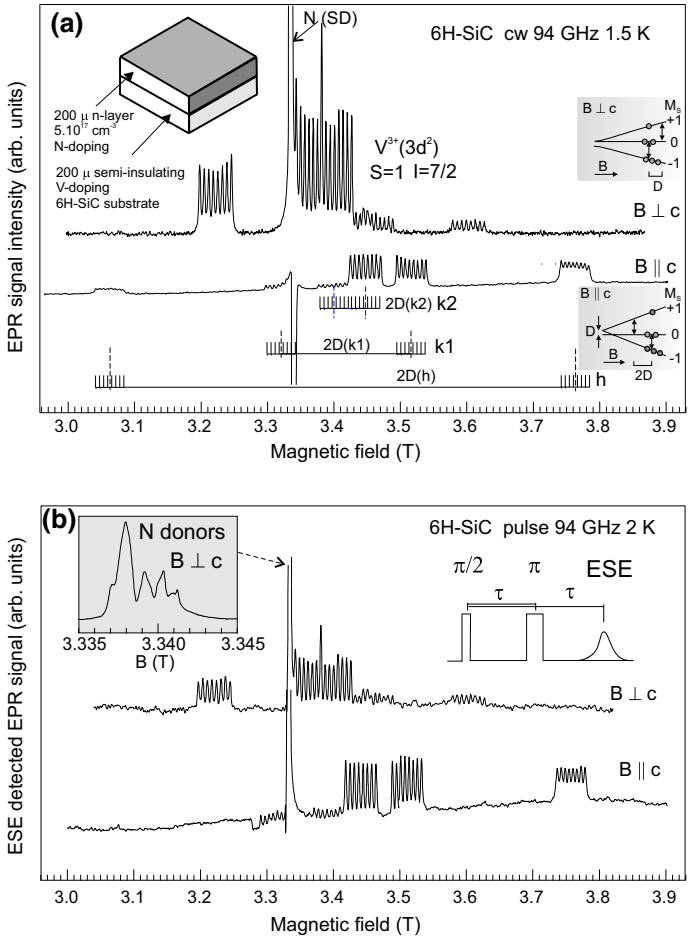

Fig. 8 **a** EPR spectra of V^{3+} ions in a 6H-SiC crystal, measured at a frequency of 94 GHz at a temperature of 1.5 K for two orientations of the magnetic field with respect to the hexagonal axis c: $B \parallel c$ and $B \perp c$. Three different positions of vanadium in the crystal are marked. The insets shows the structure of the sample (left) and the energy levels of V^{3+} (right) for $B \parallel c$ and $B \perp c$ (without the hyperfine structure splitting). The Boltzmann population distribution of the V^{3+} triplet levels is shown by circles. **b** ESE spectra of V^{3+} ions recorded at a frequency of 94 GHz at a temperature of 2 K. The inset shows the ESE spectrum of shallow nitrogen donors. The pulse sequence was $\pi/2 = 202$ ns, $\tau = 300$ ns, and $\pi = 404$ ns

at a frequency of 94 GHz and a temperature of 1.5 K for two orientations of the magnetic field with respect to the hexagonal axis c: $B \parallel c$ ($\theta = 0°$) and $B \perp c$ ($\theta = 90°$). Three different positions of vanadium in the crystal are indicated—hexagonal (h) and two quasicubic ($k1$, $k2$). The sample was a 200 μm layer of n-type 6H-SiC doped with nitrogen grown by sublimation sandwich method on a semi-insulating substrate of vanadium doped 6H-SiC (left inset in Fig. 8a). Right insets in Fig. 8a show the energy levels of V^{3+} for the two orientations; circles conditionally show the Boltzmann distribution of populations of the triplet levels at strong magnetic

fields and low temperatures. This distribution results in different intensity of fine-structure transitions and allows determining the sign of the fine-structure parameter *D*. High-frequency EPR measurements make it possible to accurately determine the spin Hamiltonian parameters, with higher order effects minimized [42]. It can be seen from Fig. 8 that the sign of *D* is positive for all positions of vanadium ions V^{3+} in SiC. In earlier works, only the absolute value of *D* was measured.

Thus, the gigantic spectral resolution of high-frequency EPR spectroscopy makes it possible to separate the positions of nitrogen donors and deeply compensating vanadium impurities in SiC crystals and silicon carbide heterostructures and clearly establish the structure of their energy levels.

ESE-detected EPR spectra of V^{3+} ions recorded at a frequency of 94 GHz in two extreme orientations at a temperature of 2 K are shown in Fig. 8b. The inset shows the spectrum of shallow nitrogen donors recorded by ESE. The pulse sequence used to detect ESE was: $\pi/2 = 202$ ns, $\tau = 300$ ns, and $\pi = 404$ ns.

4 Summary

An EPR/ESE/ODMR spectrometer was developed, operating in continuous and pulsed modes at fixed frequencies in the mm range. The flexible design of the spectrometer allows you to quickly change the configuration of the experiment. The spectrometer can be used for a study and non-destructive control of condensed materials, including nanostructured and biological objects, using EPR, photo-EPR, ESE, and ODMR. ENDOR is under development. Currently, it operates in W and D bands (at 94 and 130 GHz, respectively), but the frequency bands can be extended.

The spectrometer is based on a series of unified microwave bridges that was developed as a result of collaboration of the DOK Company and the Ioffe Institute on the same technology platform, and covers the high-frequency range up to the boundary between waveguide and quasi-optical technology. Advantages of these bridges are high stability of the output frequency, low-phase noise (narrow spectrum: better than -100 dBc at a 10 kHz offset), high output power, sensitive superheterodyne IQ receiver. Efficient and convenient microwave channel tuning system uses a variable frequency oscillator, which can also be used for operation of the spectrometer in frequency modulation mode. An original non-resonant microwave system was created to supply microwave power to the sample, which uses a circular waveguide and operates in a wide range of microwave frequencies in the 3 mm and 2 mm ranges. It does not require special tuning, and allows you quickly change the operating frequency by replacing the microwave unit and rotate the sample by rotating the circular waveguide. It is also possible to study large samples with mm sizes.

The spectrometer uses a closed-cycle magneto-optical cryogenic system with a split-coil superconducting magnet for all frequency ranges. Its operation does not depend on cryogenic infrastructure. An advantage of this system is the possibility of multiple recordings of spectra in the entire range of magnetic fields from -7 to 7 T with a smooth transition through the zero field. It provides an optical access to the sample, a wide range of the sample temperature (from 1.5 to 300 K) and high temperature stability.

The possibilities of the developed high-frequency EPR/ESE/ODMR spectrometer operating at frequencies of 94 and 130 GHz are demonstrated in measuring ODMR of NV defects in diamond, recording the EPR spectra of non-Kramers Tb^{3+} centers in YAG with a huge zero-field splitting, separating three different positions of nitrogen donors in 6H-SiC and the diagnosis of V^{3+} in SiC, the main impurity in silicon carbide used to obtain n-type materials and semi-insulating substrates.

Acknowledgements N.G.R. and A.S.G. acknowledge partial support from the Russian Foundation for Basic Research under Grant No. 19-52-12058 and Deutsche Forschungsgemeinschaft (DFG) within the framework of the ICRC project TRR 160. R.A.B. and P.G.B. acknowledge the partial support of the Russian Science Foundation (Project No. 20-12-00216) in the development of the spectrometer operating in the 2 mm range.

References

1. E.K. Zavoisky, J. Phys. (USSR) **9**, 211 (1945)
2. K. Möbius, A. Savitsky, *High-Field EPR Spectroscopy on Proteins and their Model Systems: Characterization of Transient Paramagnetic States* (Roy. Soc. Chem, Cambridge, 2008)
3. Y.S. Lebedev, in *Foundations of Modern EPR*, ed. by S.S. Eaton, K.M. Salikhov (World Scientific, Singapore, 1998), p. 731
4. Y.S. Lebedev, in *Modern Pulsed and Continuous-Wave Electro Spin Resonance*, ed. by L. Kevan, M.K. Bowman (Wiley, New York, 1990), p. 365
5. H. Blok, J.A.J.M. Disselhorst, S.B. Orlinskii, J. Schmidt, P.G. Baranov, Phys. B **340**, 1147 (2003)
6. H. Blok, J.A.J.M. Disselhorst, S.B. Orlinskii, J. Shmidt, J. Magn. Reason. **166**, 92 (2004)
7. D.E. Budil, K.A. Earle, W.B. Lynch, J.H. Freed, in *Advanced EPR Applications inBiology and Biochemistry*, ed. by A.J. Hoff (Elsevier, Amsterdam, 1989)
8. T.F. Prisner, S. Un, R.G. Griffin, Isr. J. Chem. **32**, 357 (1992)
9. M.R. Fuchs, T.F. Prisner, K. Möbius, Rev. Sci. Instrum. **70**, 3681 (1999)
10. V.F. Tarasov, G.S. Shakurov, Appl. Magn. Reson. **2**, 571 (1991)
11. J.H. Freed, Annu. Rev. Phys. Chem. **51**, 655 (2000)
12. A.K. Hassan, L.A. Pardi, J. Krzystek, A. Sienkiewicz, P. Goy, M. Rohrer, L.-C. Brunel, J. Magn. Reson. **142**, 300 (2000)
13. M. Rohrer, O. Brugmann, B. Kinzer, T.F. Prisner, Appl. Magn. Res. **21**, 257 (2001)
14. K.A. Earle, D.E. Budil, J.H. Freed, in *Advances in Magnetic and Optical Resonance*, vol. 19, ed. by W. Warren (Academic Press, New York, 1996), pp. 253–323
15. G.M. Smith, J.C.G. Lesurf, R.H. Mitchel, P.C. Riedi, Rev. Sci. Instrum. **69**, 3924 (1998)
16. J. Disselhorst, H.J. van der Meer, O.G. Poluektov, J. Schmidt, J. Magn. Reson. Ser. A **115**, 183 (1995)
17. J. Allgeier, J. Disselhorst, R. T. Weber, W.T. Wenckenbach, J. Schmidt, in *Modern Pulsed and Continuous-Wave Electron Spin Resonance*, ed. by L. Kevan, M.K. Bowman (Wiley, New York, 1990), p. 267
18. K. Möbius, W. Lubitz, A. Savitsky, Prog. Nucl. Magn. Reson. Spectrosc. **75**, 1 (2013)
19. D. Goldfarb, J. Magn. Reson. **306**, 102 (2019)
20. J. Köhler, J. Disselhorst, M. Donckers, E.J.J. Groenen, J. Schmidt, W.E. Moerner, Nature **363**, 242 (1993)
21. J. Wrachtrup, C. von Borczyskowski, J. Bernard, M. Orrit, R. Brown, Nature **363**, 244 (1993)
22. F. Jelezko, J. Wrachtrup, J. Phys. Condens. Matter **16**, R1089 (2004)
23. J. Köehler, Phys. Rep. **310**, 261 (1999)
24. A. Gruber, A. Drabenstedt, C. Tietz, L. Fleury, J. Wrachtrup, C. von Borczyskowski, Science **276**, 2012–2014 (1997)
25. P.G. Baranov, H. J. von Bardeleben, F. Jelezko, J. Wrachtrup, *Magnetic Resonance of Semiconductors and Their Nanostructures: Basic and Advanced Applications*. Springer Series in Materials Science, vol. 253 (Springer-Verlag, Wien, 2017)

26. A.I. Smirnov, T.I. Smirnova, R.L. MacArthur, J.A. Good, R. Hall, Rev. Sci. Instrum. **77**, 035108 (2006)
27. R.A. Babunts, A.G. Badalyan, N.G. Romanov, A.S. Gurin, D.O. Tolmachev, P.G. Baranov, Tech. Phys. Lett. **38**, 887 (2012)
28. R.A. Babunts, A.G. Badalyan, A.S. Gurin, B.R. Namozov, N.G. Romanov, P.G. Baranov, Tech. Phys. Lett. **43**, 389–391 (2017)
29. P.G. Baranov, R.A. Babunts, A.G. Badalyan, N.G. Romanov, L.Yu. Bogdanov, A.V. Nalivkin, RF Patent No. 2411530 (2009)
30. E.V. Edinach, Yu.A. Uspenskaya, A.S. Gurin, R.A. Babunts, H.R. Asatryan, N.G. Romanov, A.G. Badalyan, P.G. Baranov, Fiz. Tverd. Tela **61**, 1864 (2019). Phys. Solid State 61, 1820 (2019)
31. E.V. Edinach, Yu.A. Uspenskaya, A.S. Gurin, R.A. Babunts, H.R. Asatryan, N.G. Romanov, A.G. Badalyan, P.G. Baranov, Phys. Rev. B **100**, 104435 (2019)
32. R.A. Babunts, A.G. Badalyan, E.V. Edinach, A.S. Gurin, N.G. Romanov, P.G. Baranov, RF Patent No. 2711345 (2020)
33. R.A. Babunts, A.G. Badalyan, Yu.A. Uspenskaya, A.S. Gurin, N.G. Romanov, P.G. Baranov, RF Patent No. 2711228 (2020)
34. F. Jelezko, J. Wrachtrup, Phys. Stat. Sol. (a) **203**(13), 3207 (2006)
35. B.V. Yavkin, V.A. Soltamov, R.A. Babunts, A.N. Anisimov, P.G. Baranov, F.M. Shakhov, S.V. Kidalov, A.Y. Vul', G.V. Mamin, S.B. Orlinskii, Appl. Magn. Reson. **45**, 1035 (2014)
36. H.H. Woodbury, G.W. Ludwig, Phys. Rev. **124**, 1083 (1961)
37. S. Greulich-Weber, Phys. Stat. Sol. A **162**, 95 (1997)
38. E.N. Kalabukhova, N.N. Kabdin, S.N. Lukin, Sov. Phys. Solid State **29**, 8 (1987)
39. D.V. Savchenko, E.N. Kalabukhova, V.S. Kiselev, J. Hoentsch, A. Pöppl, Phys. Stat. Sol. B **246**, 1908 (2009)
40. A.V. Duijn-Arnold, R. Zondervan, J. Schmidt, P.G. Baranov, E.N. Mokhov, Phys. Rev. B **64**, 085206 (2001)
41. M.V. Muzafarova, I.V. Ilyin, A.N. Anisimov, E.N. Mokhov, V.A. Soltamov, P.G. Baranov, Phys. Solid State **58**, 2406 (2016)
42. E.V. Edinach, A.D. Krivoruchko, A.S. Gurin, M.V. Muzafarova, I.V. Ilyin, R.A. Babunts, N.G. Romanov, A.G. Badalyan, P.G. Baranov, Semiconductors **54**, 150 (2020)
43. J. Schneider, H.D. Müller, K. Maier, W. Wilkening, F. Fuchs, A. Dornen, S. Leibenzeder, R. Stein, Appl. Phys. Lett. **56**, 1184 (1990)